Available online at www.sciencedirect.com
ScienceDirect
Progress in Natural Science 19 (2009) 1003–1009
Progress in Natural Science
www.elsevier.com/locate/pnsc

Anti-saturation block adaptive quantization algorithm for SAR raw data compression over the whole set of saturation degrees

Haiming Qi *, Weidong Yu

Institute of Electronics, Chinese Academy of Sciences, Beijing 100190, China

Received 14 August 2008; received in revised form 11 September 2008; accepted 25 November 2008

Abstract

In order to improve the performance of block adaptive quantization (BAQ) when the output of the analog to digital converter (ADC) is saturated, this paper proposes an anti-saturation BAQ algorithm. First, the concept of the standard deviation of the output signal (SDOS) of the ADC is proposed. Also, unlike traditional normalization processing, SDOS is used and the mapping between SDOS and the average signal magnitude is deduced. Second, the saturation term is introduced to the Lloyd–Max quantizer and an optimal non-uniform scalar quantizer for saturated SAR raw data quantization is proposed. After this, the implementation scheme for the proposed algorithm using an FPGA is analyzed in detail. Third, the relationships among the saturation degree of the signal, the peak-to-peak value of the ADC, standard deviation of the input and output signal of the ADC and the average signal magnitude are deduced. Based on these relationships, a power compensation decoder is designed for encoding. Numerical experiment results based on ERS-1 and the simulated data show that the performance of the proposed algorithm is better than that of BAQ.

Keywords: Synthetic aperture radar (SAR); Raw data compression; Block adaptive quantization (BAQ); Anti-saturation

1. Introduction

The volume of space-borne SAR raw data is large, but both the capability for onboard data storage and the downlink bandwidth are limited. Meanwhile, with the development of modern SAR systems towards high resolution, multi-polarization, three-dimensional mapping, wide swath, multi-frequency, and multi-operation modes, the volume of SAR raw data will be even larger. Therefore, the raw data must be compressed before downlink. Compression algorithms can be divided into three categories: (i) scalar compression algorithms; (ii) vector compression algorithms; and (iii) transform domain compression algorithms. The scalar compression algorithms include block adaptive quantization (BAQ) [1], amplitude and phase (AP) [2], block floating point quantization (BFPQ) [3], fuzzy BAQ (FBAQ) [4,5], entropy-constrained BAQ (ECBAQ) [4,5], and flexible BAQ (FBAQ) [6]. The vector compression algorithms include vector quantization (VQ) [4,5], block adaptive vector quantization (BAVQ) [4,5], and trellis coded vector quantization (TCVQ) [4]. The transform domain compression algorithms include fast Fourier transform BAQ (FFT-BAQ) [4,5,7–9] and wavelet transform (WT) [4]. Although the performance of the vector compression algorithm is better than that of the scalar compression algorithm [10–12], the complexity makes it difficult to realize onboard. FFT-BAQ needs two-dimensional FFT operation and Doppler centroid estimation, so it is also very difficult to realize onboard. WT is very promising, but is also complex in realization. However, BAQ has been successfully utilized in Magellan [1], ENVISAT ASAR, TerraSAR-X and RADARSAT-2 due to its simple structure.

* Corresponding author. Tel.: +86 10 5887145 612.
E-mail address: qi_haiming@163.com (H. Qi).

1002-0071/$ - see front matter © 2009 National Natural Science Foundation of China and Chinese Academy of Sciences. Published by Elsevier Limited and Science in China Press. All rights reserved.
doi:10.1016/j.pnsc.2008.11.007

One problem must be solved in the application of BAQ, i.e. the large dynamic range of the SAR echo, which usually causes the analog-to-digital converter (ADC) to saturate [13–15]. In this scenario, the ADC output is a truncated Gaussian random signal, which does not satisfy the prerequisite of the Lloyd–Max quantizer [16,17] and the BAQ performance deteriorates. Ref. [18] used conventional BAQ and low compression ratio (CR) BAQ to compress low SD signals and high SD signals, respectively. This approach suffers in that the data forming system onboard is more complicated, and the judgment operation has additional cost for the low SD signal. Meanwhile, low CR BAQ increases the bandwidth of the downlink data, and the uncertainty of SD leads to uncertainty of the bandwidth of the downlink data. These drawbacks make this approach unfeasible in practice.

The key points of the saturation problem are as follows. First, the truncation effect of the ADC invalidates the mapping between the average signal magnitude (ASM) and the standard deviation of the input signal (SDIS) to the ADC. Second, the output signal of the ADC with truncation effect does not obey a Gaussian distribution. Thus the prerequisite of the Lloyd–Max quantizer is not satisfied, which causes the BAQ performance to deteriorate. This paper proposes a new mapping between ASM and the standard deviation of the output signal (SDOS) from the ADC and the optimal non-uniform scalar quantizer (ONSQ) in order to solve these two issues.

2. Mapping between ASM and SDOS from ADC

The SAR echo can be viewed as a superposition of the responses of many small scatterers in each azimuth and range resolution cell. Based on the central limit theorem, both the in-phase and quadrature components satisfy a Gaussian distribution. The amplitude has a Rayleigh distribution and the phase is normally distributed at the interval $[-\pi,\pi]$. The prerequisite of the Lloyd–Max quantizer is that the input signal of the quantizer must satisfy a standard Gaussian distribution, so SAR raw data must be normalized before quantization. For simple implementation in engineering, the mapping between the ASM and the SDIS is utilized to estimate the SDIS. Ref. [1] gives the mapping between ASM and SDIS as Eq. (1)

$$|\overline{I}| = |\overline{Q}| = 127.5 - \sum_{n=0}^{127} \mathrm{erf}\left(\frac{n+1}{\sqrt{2}\sigma}\right) \tag{1}$$

where $\mathrm{erf}(x) = \frac{2}{\sqrt{\pi}} \int_0^x \exp(-t^2)\,\mathrm{d}t$ and σ is the SDIS to ADC mapping.

Eq. (1) assumes that an 8-bit ADC is used to quantize the SAR raw data. However, when the ADC is heavily saturated, the output power of the ADC suffers losses. Thus using SDIS to ADC cannot effectively normalize the saturated SAR raw data. Here, we formulate the mapping between ASM and SDOS from the ADC and use it to normalize the saturated SAR raw data. The procedure of the deduction is available in Appendix A.

The SDOS from ADC can be obtained from Eq. (2) as

$$\sqrt{Dx} = \sqrt{\sum_{n=0}^{126}(n+0.5)^2\left[\mathrm{erf}\left(\frac{n+1}{\sqrt{2}\sigma}\right) - \mathrm{erf}\left(\frac{n}{\sqrt{2}\sigma}\right)\right] + (127.5)^2\left[1 - \mathrm{erf}\left(\frac{127}{\sqrt{2}\sigma}\right)\right]} \tag{2}$$

From Eqs. (2) and (1), we can obtain the implicit function between the ASM and the SDOS of the ADC. Fig. 1 shows the mapping between the ASM and SDOS of the ADC compared with the mapping between the ASM and SDIS to ADC. From Fig. 1, we can see that the linear parts of these two curves are nearly overlapped and the signs of the first-order derivatives of the nonlinear parts of these two curves are opposite.

3. Anti-saturation optimal non-uniform scalar quantizer

3.1. Principle of the Lloyd–Max quantizer

The Lloyd–Max quantizer is the optimal non-uniform scalar quantizer for standard Gaussian distributed signal quantization. It was proposed by Max [16] and Lloyd [17] independently and has been improved by other researchers [19–25].

Ref. [16] defined the distortion D between the input signal and the output signal as

$$D = \mathrm{E}\left[(s_{\mathrm{in}} s_{\mathrm{out}})^2\right] = \sum_{i=1}^{N} \int_{x_i}^{x_{i+1}} (x - y_i)^2 f(x)\,\mathrm{d}x \tag{3}$$

where s_{in} and s_{out} are the input signal and the output signal, respectively. $f(x)$ is the amplitude probability density function of the input signal. $x_{N+1} = \infty$, $x_1 = -\infty$, and the convention is that an input between x_i and x_{i+1} has a corresponding output y_i.

Then, if the differential coefficient of D with respect to the x_i's and y_i's equals zero, we derive the minimum of D as

$$\frac{\partial D}{\partial x_j} = (x_j - y_{j-1})^2 f(x_j) - (x_j - y_j)^2 f(x_j) = 0 \quad j = 2,\ldots,N \tag{4}$$

$$\frac{\partial D}{\partial y_j} = -\int_{x_j}^{x_{j+1}} (x - y_j) f(x)\,\mathrm{d}x = 0 \quad j = 1,\ldots,N \tag{5}$$

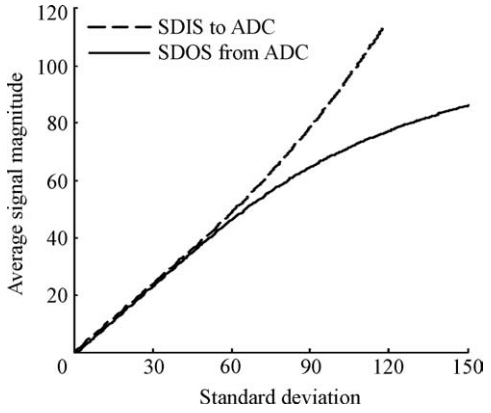

Fig. 1. Comparison of the mapping between ASM and SDIS with that between ASM and SDOS.

The iterative conditions can be deduced from Eqs. (4) and (5) as

$$\left.\begin{array}{ll} x_j = \frac{y_j + y_{j-1}}{2}, & j = 2, \ldots, N \\ \int_{x_j}^{x_{j+1}} (x - y_j) f(x)\,\mathrm{d}x = 0, & j = 1, \ldots, N \end{array}\right\} \quad (6)$$

If y_j satisfies the second formula of Eq. (6), we call it the centroid of the area of $f(x)$ between x_j and x_{j+1}. When y_N is the centroid of the last interval of x, Eq. (6) is solved [16].

When the ADC is saturated, the output signal of the ADC with truncation effect does not obey a Gaussian distribution. The iterative conditions must be modified accordingly.

3.2. Principle of the optimal non-uniform scalar quantizer

Obviously, the probability density function of the unsaturated part does not change before or after the ADC. So the numerical approach is the same as that discussed in Section 3.1, except that the centroid condition should be modified. The centroid condition in the last interval can be described as

$$\int_{x_L}^{\infty} (x - y_L) f(x)\,\mathrm{d}x = 0 \quad (7)$$

where x_L and y_L are the transition point and the reconstruction point in the last interval. Eq. (7) can be further rewritten as

$$\int_{x_L}^{M} (x - y_L) f(x) dx + \int_{M}^{\infty} (x - y_L) f(x)\mathrm{d}x = 0 \quad (8)$$

Taking the saturation into account, Eq. (8) can be deduced as

$$\int_{x_L}^{M} (x - y_L) f(x)\,\mathrm{d}x + (M - y_L) \int_{M^-}^{M^+} p(x)\,\mathrm{d}x = 0 \quad (9)$$

where $P(x)$ is the probability density function of the saturated signal on the truncated point.

The integral interval $[M^-, M^+]$ is the nearest neighborhood of M. The first part and the second part of Eq. (9) represent the unsaturated and the saturated sections in the last interval, respectively.

Since the probability of the interval beyond the truncated point in Eq. (8) equals that on the truncated point in Eq. (9), we can rewrite Eq. (9) as

$$\int_{x_L}^{M} (x - y_L) f(x)\mathrm{d}x + (M - y_L) \int_{M}^{\infty} f(x)\mathrm{d}x = 0 \quad (10)$$

Eq. (10) is solvable compared with Eq. (9), and the latter is just a mathematical representation. The flow chart of anti-saturation ONSQ is shown in Fig. 2.

4. Encoding and decoding scheme

4.1. Introduction

Fig. 3 shows the encoding and decoding scheme of BAQ and of the proposed algorithm. The solid lines indicate the same processes and the dashed lines show the different processes.

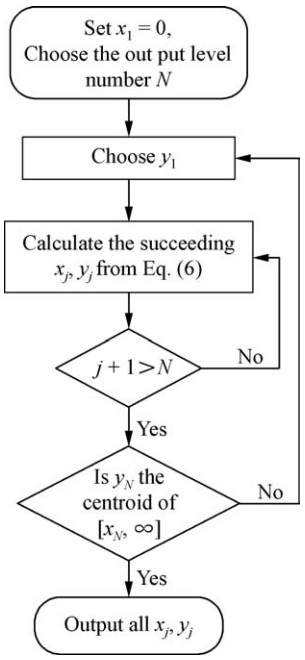

Fig. 2. The flow chart of anti-saturation ONSQ.

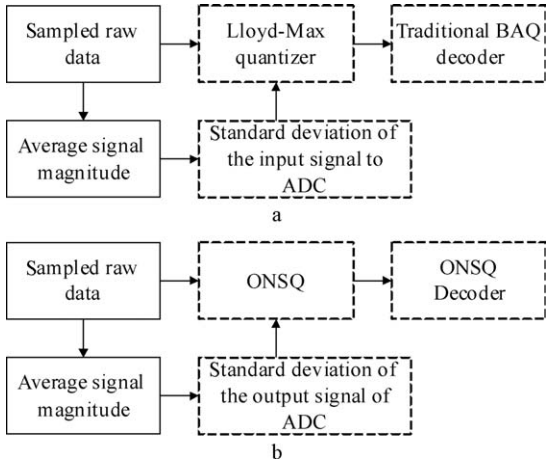

Fig. 3. Encoding and decoding scheme of BAQ and the proposed algorithm. (a) Encoding and decoding scheme of BAQ; (b) encoding and decoding scheme of the proposed algorithm.

From Fig. 2, we can see that the proposed algorithm utilizes the SDOS rather than the SDIS to normalize the sampled raw data. In the quantization procedure, the proposed algorithm uses anti-saturation ONSQ instead of the Lloyd–Max quantizer to quantize the saturated SAR raw data. As for the decoding procedure, this paper proposes the power loss compensation decoder (PLCD) to compensate for the power loss due to ADC saturation.

4.2. Encoding scheme

Considering the implementation complexity, the encoding scheme proposed here is very simple. We only need to update the look-up-table (LUT) saved in the field programmable

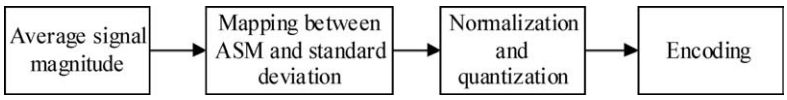

Fig. 4. The design flow of the LUT.

gate array (FPGA) chip and do not need to update the Verilog HDL script or any hardware configuration.

Fig. 4 outlines the design flow of the LUT.

From Fig. 4, we can draw the conclusion that the design flow of the LUT mainly contains three steps, which are mapping between the ASM and the standard deviation, normalization and quantization, and encoding. The ASM is calculated by an accumulator array. Then, taking the normalization and quantization as the transition, there is a mapping between the ASM and the encoding results. This mapping is the core procedure of the LUT. As for the quantization process, the Lloyd–Max quantizer and the anti-saturation ONSQ are the optimal quantizers for low and high SD SAR raw data, respectively. So, we can save the encoding results of the BAQ and anti-saturation ONAQ in the low and high addresses of the LUT accordingly. Then the LUT can output optimal quantization results adaptively according to the variance of the ASM. More details can be found in Ref. [26].

4.3. Decoding scheme

The definition of the saturation degree is

$$SD = \frac{NUM_{\text{satu}}}{NUM_{\text{total}}} \times 100\% \tag{11}$$

where NUM_{satu} is the number of saturated samples, and NUM_{total} is the total number of samples.

We can extend this definition to successive random variables, and then we can obtain

$$SD = 2\int_{M}^{\infty} f(x)\,\mathrm{d}x \tag{12}$$

where $f(x)$ is the probability density function of the SAR raw data.

Obviously, when the SAR raw data obey a Gaussian distribution, we can obtain the relationships between the saturation degree, the peak-to-peak value of the ADC and the SDIS from Eq. (12). These relationships are shown in Fig. 5.

From Fig. 5, we can see that when choosing certain peak-to-peak values of the ADC, the saturation degree monotonously nonlinearly increases as the SDIS goes up. However, when SDIS is fixed, the relationship between the saturation degree and the peak-to-peak value of the ADC is inverted.

Also, from Eqs. (1), (2), and (12), we obtain the relationships between the saturation degree, the peak-to-peak value of the ADC, the SDIS, the ASM and the SDOS as shown in Fig. 6.

As can be seen in Fig. 6, the solid lines and the dashed lines depict the explicit and implicit functions, respectively. The saturation of the ADC will cause power losses for the

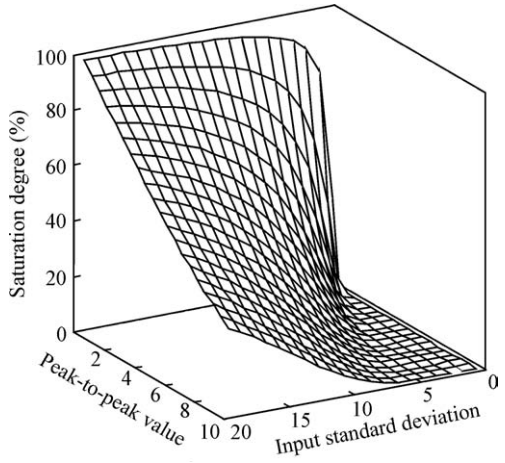

Fig. 5. The relationships between saturation degree, peak-to-peak value of ADC and SDIS.

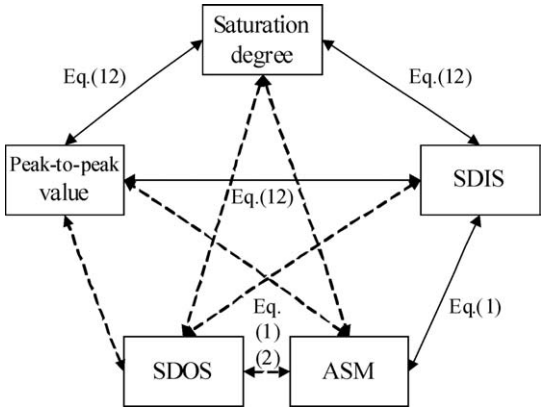

Fig. 6. The relationships between five parameters.

input signal [13–15], so when we decode, compensation should be considered for this power loss. The decoding procedure is as follows. First, we decode according to the anti-saturation ONSQ and the LUT, and then use the SDIS to compensate for the power loss of the input signal.

5. Numerical experiment

5.1. Simulation of the whole set of saturation of raw data domain

The peak-to-peak value of the ADC is 2 V in this simulation. The CR is 8/3. The simulation result is shown in Fig. 7.

As shown in Fig. 7, on the left side of the dividing line of the high and low addresses, the SNR is almost the same; this is because the low address of the LUT stores BAQ

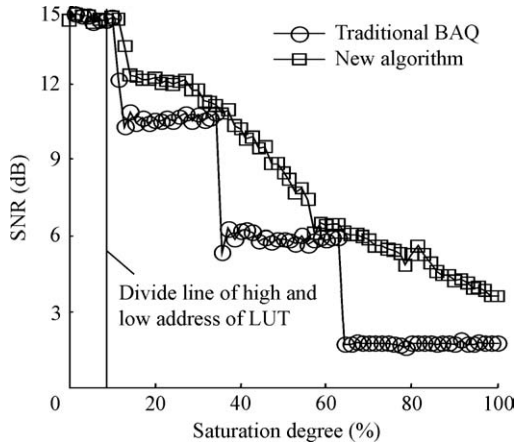

Fig. 7. Raw data domain SNR of BAQ and that of the proposed algorithm.

Table 1
Parameters of ERS-1 data used in this paper.

Scene	Orbit	Frame	Observation time	Look angle at center swatch (°)
Greenland	ERS1: 23846	2259	1996.2.05	23.817

codes. However, beyond the dividing line of the high and low addresses, the performance of the proposed algorithm is much better than that of BAQ. The reason is that ONSQ rather than the Lloyd–Max quantizer is the optimal scalar quantizer for the saturated Gaussian signal.

5.2. The results of the real SAR raw data

The following results are based on ERS-1 data from the European Space Agency (ESA), and the parameters are listed in Table 1.

Fig. 8 shows the images of two typical areas chosen in this study. The size of these two images is 4096×768 (range $\times$ azimuth). The white floccule seen in Fig. 8 is snow in Greenland. Here we set the range direction of the image into eight sub-blocks equally, i.e. the size of each sub-block is 512×768. The SD of each sub-block and raw data domain SNR is depicted in Fig. 9.

Fig. 9(a) shows the saturation degree of each sub-block. The saturation degree of the eighth sub-block is on the left side of the dividing line of the high and low addresses of the LUT. So, the Lloyd–Max quantizer is the optimal one for this sub-block. Fig. 9(b) and (c) shows the performances of BAQ and the proposed algorithm based on image 1. The difference between Fig. 9(b) and (c) is that the 8th sub-block is quantized by the Lloyd–Max quantizer. If we do not use the left side of the dividing line of the high and low addresses of the LUT, then the performance will deteriorate as shown in Fig. 9(b). From Fig. 9(c) and (d) we can conclude that the performance of the proposed algorithm is much better than that of BAQ over the whole set of SD.

Here it is worth noting that the ranges of SNR shown in Figs. 7 and 9 are not exactly the same, because Fig. 7 is the result of simulation data while Fig. 9 is that of the real data, respectively. When we calculate the SNR, the ideal signal in Fig. 7 is the input signal to the ADC, but the signal in Fig. 9 is the output signal from the ADC. The latter is quantized and saturated. This difference causes the different SNR ranges. So, there is no means to compare SNRs of different real data sets according to the compression algorithm. As for real data, we should compare SNRs of different compression algorithms according to a certain real data set.

6. Conclusions

This paper proposes an anti-saturation block adaptive quantization algorithm for saturated SAR raw data compression. Numerical experiments based on simulation and real SAR raw data show that the performance of the proposed algorithm is much better than that of BAQ over the

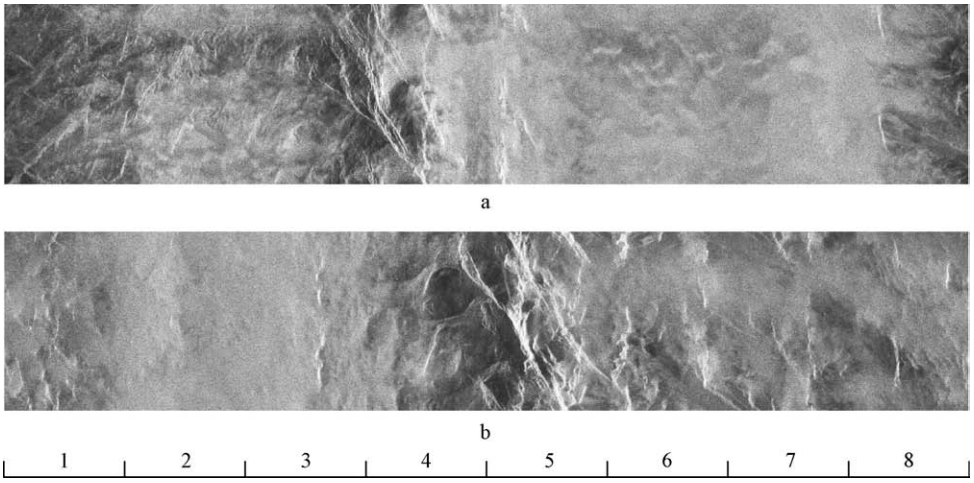

Fig. 8. Two typical areas and the sub-blocks partition. (a) Image 1; (b) image 2.

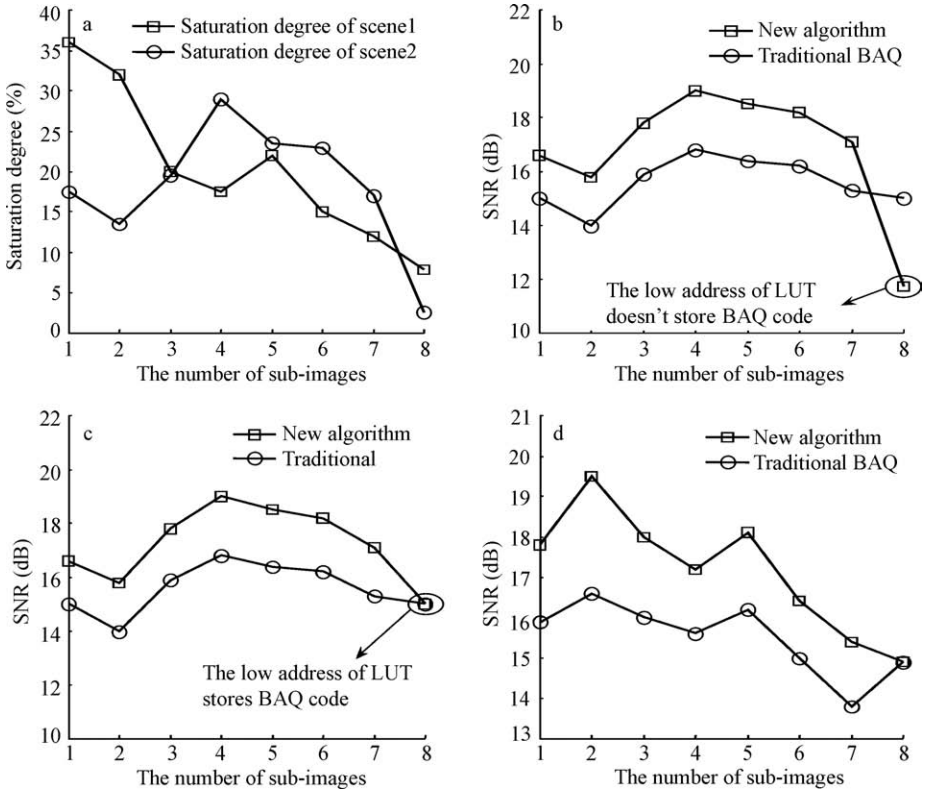

Fig. 9. Experimental results of real SAR raw data. (a) SD curves of image 1 and image 2; (b) SNR of the proposed algorithm (does not store BAQ code in the low address of LUT) compared with that of BAQ utilizing real data set 1; (c) SNR of the proposed algorithm compared with that of BAQ utilizing real data set 1; (d) SNR of the proposed algorithm compared with that of BAQ utilizing real data set 2.

whole set of saturation degrees. The implementation of the proposed algorithm is very simple and can be easily utilized in application.

Acknowledgements

This work was supported by Knowledge Innovation Project of Chinese Academy of Sciences (Grant No. KGCX2-YW-412). Chinese Academy of Sciences (Grant No. KGCX2-YW-412). We also appreciate the help from Prof. Wang Guiying, Dr. Wang Shuo and Dr. Li Xin on the modification of this paper.

Appendix A. The relationship between ASM and SDOS

The assumption in Ref. [1] is

$$|\bar{I}| = |\overline{Q}| = 2\sum_{n=0}^{N-1}(x_n + 0.5)\int_{x_n}^{x_{n+1}} p(x)\,\mathrm{d}x \tag{A1}$$

where σ is the SDIS to ADC. $p(x)$ is the probability density function of Gaussian distribution.

$$P(x) = \frac{1}{\sqrt{2\pi}\sigma}\exp\left(-\frac{x^2}{2\sigma^2}\right) \tag{A2}$$

Considering the saturation items in Eq. (A2),

$$|\bar{I}| = |\overline{Q}| = 2\sum_{n=0}^{N-1}(x_n + 0.5)\int_{x_n}^{x_{n+1}} p(x)dx + 2\left[(x_N + 0.5)\int_{x_N}^{\infty} p(x)dx\right] \tag{A3}$$

where the term $2[(x_{N-1}+0.5)\int_{x_N}^{\infty} p(x)\,\mathrm{d}x]$ represents the output signal when the input signal is at the interval $[x_N, \infty]$ and $[-\infty, -x_N]$. Then,

$$Dx = Ex^2 - (Ex)^2 \tag{A4}$$

Since the SAR raw data has a zero mean Gaussian distribution, so $Ex = 0$. Then,

$$\begin{aligned} Dx = Ex^2 &= 2\sum_{n=0}^{N-1}(x_n+0.5)^2\int_{x_n}^{x_{n+1}} p(x)\,\mathrm{d}x + 2\left[(x_{N+0.5})^2\int_{x_N}^{\infty} p(x)\,\mathrm{d}x\right] \\ &= \sum_{n=0}^{126}(x_n+0.5)^2\left[\mathrm{erf}\left(\frac{x_{n+1}}{\sqrt{2}\sigma}\right) - \mathrm{erf}\left(\frac{x_n}{\sqrt{2}\sigma}\right)\right] \\ &\quad + (127.5)^2\left[\mathrm{erf}(\infty) - \mathrm{erf}\left(\frac{127}{\sqrt{2}\sigma}\right)\right] \\ &= \sum_{n=0}^{126}(n+0.5)^2\left[\mathrm{erf}\left(\frac{n+1}{\sqrt{2}\sigma}\right) - \mathrm{erf}\left(\frac{n}{\sqrt{2}\sigma}\right)\right] \\ &\quad + (127.5)^2\left[1 - \mathrm{erf}\left(\frac{127}{\sqrt{2}\sigma}\right)\right] \end{aligned} \tag{A5}$$

So, the SDOS is

$$\sqrt{Dx} = \sqrt{\sum_{n=0}^{126}(n+0.5)^2\left[\mathrm{erf}\left(\frac{n+1}{\sqrt{2}\sigma}\right) - \mathrm{erf}\left(\frac{n}{\sqrt{2}\sigma}\right)\right] + (127.5)^2\left[1 - \mathrm{erf}\left(\frac{127}{\sqrt{2}\sigma}\right)\right]} \tag{A6}$$

References

[1] Kwok R, Johnson WT. Block adaptive quantization of Magellan SAR data. IEEE Trans Geosci Remote Sensing 1989;27(4):375–83.

[2] Yao SC, Wang YF, Zhang BC, et al. Amplitude and phase compression algorithm for SAR raw data. J Electr Inform Technol 2002;24(11):1627–33.

[3] Pan ZG. The study of data compression algorithm for synthetic aperture radar at low bit rate. Ph.D. Dissertation. Institute of Electronics, Chinese Academy of Sciences; 2006.

[4] Jordan RL, Huneycutt BL. The SIR-C/X-SAR synthetic aperture radar system. IEEE Trans Geosci Remote Sensing 1995;33(4):829–39.

[5] Boustani AE, Branham K, Kinsner W. A review of current raw SAR data compression. In: Canadian conference on electrical and computer engineering. Toronto, Canada; 2001.

[6] Benz U, Strodl K, Moreria A. A comparison of several algorithms for SAR raw data compression. IEEE Trans Geosci Remote Sensing 1994;33(5):1266–76.

[7] Kuduvalli G, Dutkiewicz M, Cumming I. Synthetic aperture radar signal data compression using block adaptive quantization. In: GSFC space earth science data compression conference. Goddard Space Flight Center, USA; 1994.

[8] Fischer J, Benz U, Moreira A. Efficient SAR raw data compression in frequency domain. In: Proceedings IGARSS'99. Hamburg, Germany; 1999.

[9] Yang YZ, Huang SJ, Wang JG. Frequency region quantization coding method research for SAR raw data. System Eng Electr 2005;27(12):2107–11.

[10] Guan ZH, Zhu ZD, Zhu DY. SAR raw data compression using vector quantization techniques. J Nanjing Univ Sci Technol 2006;30(2):157–61.

[11] Guan ZH, Zhu ZD, Zhu DY. Compression of SAR raw data by block adaptive quantization spherical vector quantization. ACTA Aeronaut Astronaut Sin 2005;27(1):82–6.

[12] Guan ZH, Zhu DY, Zhu ZD. Compression of SAR raw data with normalized adaptive predictive vector quantization. J Electr Inform Technol 2006;28(3):507–11.

[13] Shimada M. Radiometric correction of saturated SAR data. IEEE Trans Geosci Remote Sensing 1999;37(1):467–78.

[14] Nicoll J, Gens R, Denny P. Pre-processing compensation for saturation power loss in SAR data. In: Proceedings IGARSS. Fairbanks, USA; 2002.

[15] Hu DH, Zhou HX, Hong W. Correction method for saturated SAR data to improve radiometric accuracy. In: Proceedings IGARSS. Seoul, South Korea; 2005.

[16] Max J. Quantizing for minimum distortion. IRE Trans Theory 1960;IT-6:7–12.

[17] Lloyd S. Least squares quantization in PCM. IEEE Trans Inform Theory 1982;28(2):129–37.

[18] Zhao YP, Wan F, Lei H. Compression on fractional saturation SAR raw data. J Electr Inform Technol 2004;26(3):489–94.

[19] Wu XL. On initialization of Max's algorithm for optimum quantization. IEEE Trans Commun 1990;38(10):1653–6.

[20] Cheung MY, Vaisey J. A comparison of scalar quantization strategies for noisy channel data transmission. IEEE Trans Commun 1995;43(2):732–42.

[21] Koren Y, Yavneh I, Spira A. A multigrid approach to the scalar quantization problem. IEEE Trans Inform Theory 2005;51(8):2993–8.

[22] Trushkin AV. On the design of an optimal quantizer. IEEE Trans Inform Theory 1993;39(4):1180–94.

[23] Ortega A, Vetterli M. Adaptive scalar quantization without side information. IEEE Trans Image Process 1997;6(5):665–76.

[24] Strintzis MG, Tzovaras D. Optimal construction of subband coders using Lloyd–Max quantizers. IEEE Trans Image Process 1998;7(5):649–67.

[25] Chang TC, Allebach JP. Quantization of accumulated diffused errors in error diffusion. IEEE Trans Image Process 2005;14(12):1960–76.

[26] Qi H. China Patent 200710122471.X; 2007.